Chlorin-based symmetrical and unsymmetrical dimers with amide linkages: effect of the substituents on photodynamic and photophysical properties

Gang Zheng,[a] Mohammad Aoudia,[b,c] David Lee,[d] Michael A. Rodgers,[b] Kevin M. Smith,[d] Thomas J. Dougherty[a] and Ravindra K. Pandey *[a,e]

[a] *Chemistry Section, Photodynamic Therapy Center, Roswell Park Cancer Institute, Buffalo, NY 14263, USA*
[b] *Center for Photochemical Sciences, Bowling Green State University, Bowling Green, Ohio 43403, USA*
[c] *Sultan Qaboos University, College of Science, Chemistry Department, P.O. Box 36, Al-Khod 123, Sultanate of Oman, Oman*
[d] *Department of Chemistry, University of California, Davis, CA 95616, USA*
[e] *Department of Nuclear Medicine, Roswell Park Cancer Institute, Buffalo, NY 14263, USA. E-mail: ravindra.pandey@roswellpark.org*

Received (in Cambridge, UK) 26th April 2000, Accepted 28th July 2000
Published on the Web 1st September 2000

In this study, we report syntheses, *in vivo* biological activity, and photophysical properties of a series of chlorin-based symmetrical and unsymmetrical dimers with amide linkages. All compounds exhibited strong absorption maxima at wavelengths ranging between λ_{max} 660 and 702 nm. Compared with the formylpyropheophorbide *a* dimer **7** and purpurin 18 dimer **9** containing electron-withdrawing substituents at peripheral positions, pyropheophorbide *a* dimer **6**, 3-devinyl-3-(1-hexyloxyethyl)pyropheophorbide *a* dimer **8**, and unsymmetrical dimer **12** in which the chlorin e_6 and 3-devinyl-3-(1-hexyloxyethyl)pyropheophorbide *a* moieties are linked with amide bonds, produced high fluorescence yields. For all photosensitizers, energy transfer from the sensitizer triplet to the ground state of oxygen is irreversible with rate constants $k_{T\Sigma} \approx 2 \times 10^9$ M^{-1} s^{-1}, a value in the diffusion-limited rate range. This energy transfer resulted in relatively high singlet oxygen quantum yields ($\Phi_\Delta \approx 0.50$ for compounds **12** and **8**; and $\Phi_\Delta \approx 0.30$ for compounds **6** and **7**). Among these dimers, compound **9** with a six-membered anhydride ring system produced the lowest singlet oxygen quantum yield (Φ_Δ 0.06). The *in vivo* PDT efficacy of these compounds was evaluated in DBA/2 mice bearing SMT/F tumors. Among all the dimers, the unsymmetrical dimer **12** was found to be most effective, but it was significantly less active than the related monomer 3-devinyl-3-(1-hexyloxyethyl)pyropheophorbide *a* **2**.

Introduction

In recent years porphyrin-based photosensitizers have experienced enormous interest due to their potential use in photodynamic therapy (PDT).[1] These compounds are believed to kill tumors both by direct action on the tumor cells and by destroying the blood supply to the malignant cells, which ultimately starves the tumor of oxygen and nutrients.[2] As the tumor breaks down, the tumor site becomes inflamed, and this helps stimulate the body's immune response, speeding up the tumor's destruction. Mechanisms of tumor death include both tumor-cell necrosis and apoptosis.[1] Currently, a major objective of various investigators has been to design photosensitizers with improved tumor selectivity. This will help to reduce the skin phototoxicity, the main drawback associated with Photofrin®, a purified form of haematoporphyrin derivative (HPD), which consists of a mixture of various dimers and higher oligomers with ether, ester and carbon–carbon linkages.[3]

The other drawback associated with Photofrin® and other porphyrin-based photosensitizers is related to their weak absorption in the long-wavelength region. It is well established that both absorption and scattering of light by tissue increases as the wavelength decreases, and that the most efficient sensitizers are those that have strong absorption bands between 700 and 800 nm.[4] Haem proteins in tissue account for most of the tissue-related absorption of light in the visible region. Light penetration drops off rapidly below 550 nm; however, it doubles from 550–630 nm (where Photofrin® is activated) and doubles again in going to 700 nm.[1] This is followed by a 10% increase in tissue penetration as the wavelength moves towards 800 nm. Therefore, the emphasis for development of new drugs has been concentrated on chlorin- and bacteriochlorin-related compounds.

In an effort to characterize Photofrin® we and others have previously reported the synthesis and biological activity of various porphyrin dimers and higher oligomers joined with ether, ester and carbon–carbon linkages.[5] The biological activity of these oligomers was compared with that of the related monomers, and it was interesting to observe that most of the monomers which were biologically inactive when converted into dimers with ether and carbon–carbon linkages showed enhanced PDT efficacy.[6,7] Besides the linkages, the overall lipophilicity and the presence and position of the substituents in the molecule also played a significant role in PDT response. Under physiological conditions, porphyrin dimers and trimers with ester linkages were found to be unstable with limited photosensitizing efficacy.[5b]

In our goal to develop more effective photosensitizers, one of our objectives has been to establish structure–activity relationships among a variety of long-wavelength-absorbing chlorin- and bacteriochlorin-based compounds.[8,9] A few years ago, Ando *et al.*[10a] showed that chlorin *e*, which is inactive *in*

DOI: 10.1039/b003367g

vivo, showed improved activity on conversion into the corresponding dimer and trimer with amide linkages. We were interested to extend this approach further to examine the effect of a variety of substituents among chlorin-based dimers with amide linkages, and to investigate their influence on photophysical and photobiological properties.

Results and discussion

For our studies pyropheophorbide *a* **1**, 3-devinyl-3-(1-hexyloxyethyl)pyropheophorbide *a* (HPPH) **2**, 3-devinyl-3-formylpyropheophorbide *a* **3**, chlorin e_6 13^1,15^2-dimethyl ester **4** and purpurin 18 **5** were used as substrates.[1] These compounds were chosen due to their promising absorption and lipophilic characteristics. For example: chlorins **1**, **2** and **4** exhibit long-wavelength absorption near 665 nm, but differ in their lipophilic characteristics and were reported to be effective *in vitro*. Chlorins **1** and **4** at low doses did not demonstrate any PDT efficacy in mice; at high doses (5 mg kg^{-1}) after light treatment at appropriate wavelengths, these compounds were found to be toxic. On the other hand, the hexyl ether derivative of pyropheophorbide *a* (HPPH) **2** was found to be extremely effective at a low dose of 0.3 mg kg^{-1} when treated with light at 24 h post injection of the drug.[8,9] This drug is currently in Phase I/II human clinical trials at Roswell Park Cancer Institute, Buffalo for the treatment of various types of tumors. Chlorin **3**, in which the vinyl group is replaced with a formyl substituent, produced a red shift of 30 nm with long-wavelength absorption near 690 nm. In preliminary screening, compared with the parent analogue **1**, the formylpyropheophorbide **3** showed significant PDT efficacy (67% tumor response at day 7 at a dose of 2.5 mg kg^{-1}). Purpurin 18 **5**, which has also been reported as an active photosensitizer *in vitro* by Hoober *et al.*,[11] did not show any *in vivo* efficacy under similar treatment conditions or at higher drug doses. For comparative *in vivo* studies, our next step was to convert these monomers into related dimers joined with amide linkages. These studies were performed to investigate if an ineffective compound can be converted into an active drug, and if the photosensitizing activity of the effective monomers could further be improved.

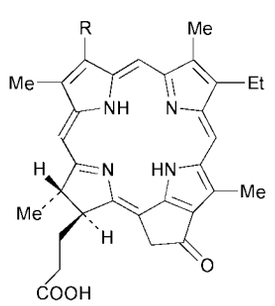

1. R = CH=CH_2
2. R = CH(O-hexyl)Me

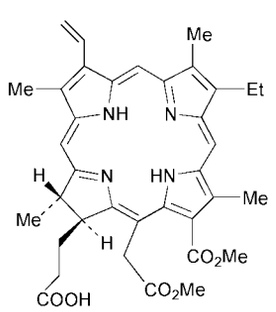

4

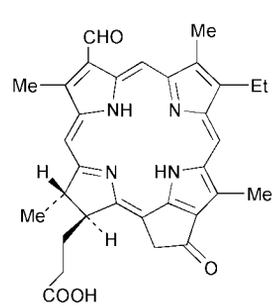

3

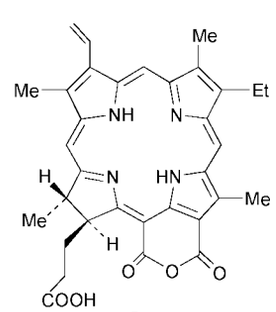

5

Based on this rationale, a series of symmetrical and unsymmetrical dimers **6**–**9** and **12** joined by an amide linkage were synthesized (Schemes 1 and 2). In brief, for the preparation of symmetrical dimers **6**, **8** and **9**, pyropheophorbide *a* **1**, 3-devinyl-3-(1-hexyloxyethyl)pyropheophorbide *a* (HPPH) **2**, and purpurin 18 **5**, were individually allowed to react with DCC, L-lysine and DMAP at room temperature, and the corresponding dimers were obtained in 62–72% yield. The structures of the newly synthesized compounds were confirmed by NMR and mass spectroscopy. The ^{1}H NMR spectrum of lysine-bridged HPPH dimer **8** showed a very complicated pattern because of the presence of asymmetric centers. When $CDCl_3$ alone was used as the NMR solvent, two sets of resonances for *meso*-protons (5-H, 10-H and 20-H) at δ 9.74 (× 2 *meso*-H), 8.48 (× 2 *meso*-H), 8.25 (× 1 *meso*-H) and 8.03 (× 1 *meso*-H) were observed. However, severe aggregation led to poor resolution. When 5 μL of pyridine-d_5 was added, all signals were much better resolved. For example, the multiplet at δ 9.74 (2 *meso*-H) appeared as two sets of singlets at δ 9.75, 9.73 and 9.71, 9.69, indicating the presence of diastereomers. For the preparation of the related 3-formyl analogue, pyropheophorbide *a* methyl ester was treated with osmium tetraoxide/sodium periodate to produce the related 3-formyl analog **3** in 66% yield, with long-wavelength absorption at 698 nm. Reaction with **3** with DCC, L-lysine and DMAP produced the corresponding dimer **7** in 60% yield. In the NMR spectrum, the absence of the vinyl resonances at δ 7.74, 7.66, 6.20, 6.10, the presence of the formyl resonances at δ 11.27 and 11.05, as well as the data obtained from combustion analysis confirmed the dimeric structure **7**.

For the preparation of unsymmetrical dimer **12**, pheophorbide *a* methyl ester **10** was treated with propane-1,3-diamine and the intermediate amine **11** was isolated in 79% yield. Reaction of amine **11** with HPPH **2** under similar reaction conditions as discussed for the preparation of symmetrical dimers produced unsymmetrical dimer **12** in 70% yield. The structure of dimer **12** was confirmed by ^{1}H NMR, ^{13}C NMR and mass spectroscopy (see Experimental section). The ^{13}C NMR spectrum of dimer **12** showed a total of 78 peaks which clearly revealed its unsymmetrical nature. However, the *R*/*S* isomeric nature due to the presence of the hexyl ether functionality was not distinguishable. Unlike that of most symmetrical dimers, the ^{1}H NMR spectrum of dimer **12** was much more complicated. However, the distinctive resolution of all the proton resonances in the NMR spectrum of dimer **12** enabled us to assign all the peaks by their through-space interactions and coupling patterns obtained by 2D/ROESY and COSY studies (Fig. 1). The results are summarized in Table 1. Some noteworthy features were as follows: as shown in Fig. 1, the asymmetrical center at position 3^1 of the HPPH macrocycle (ring A) clearly induces the split of the adjacent *meso*-proton [5-H(A)] signal appearing at δ 9.68 and 10-H(A) at δ 9.21, whereas the rest of resonances from *meso*-protons [10-H(B), 5-H(B), 20-H(B) and 20-H(A)] appeared as singlets at δ 9.47, 9.40, 8.66 and 8.37. Besides, the 3^1 chiral center is also responsible for the splitting of adjacent 3^1-H(A) at δ 5.80 and 7-Me(A) at δ 3.15.

Comparative *in vivo* photosensitizing efficacy

The *in vivo* photosensitizing ability of the monomeric and dimeric analogues was evaluated in mice (DBA/2) transplanted with SMT/F tumor by following the standard methodology.[12] The biological activity of monomeric chlorins **1**–**5** was compared with that of the corresponding dimers **6**–**9** and **12** (Table 2). Among all the monomers, HPPH **2** was found to be most effective, at a dose of 0.4 and 1.0 μmol kg^{-1} with 60% and 100% tumor control on day 30 respectively. The related formyl analogue **3** and chorin e_6 dimethyl ester **4** at similar drug doses were not effective. At a higher dose (4.0 μmol kg^{-1}) these compounds were found to be toxic after photic treatment. The formylpyropheophorbide **3** with long-wavelength absorp-

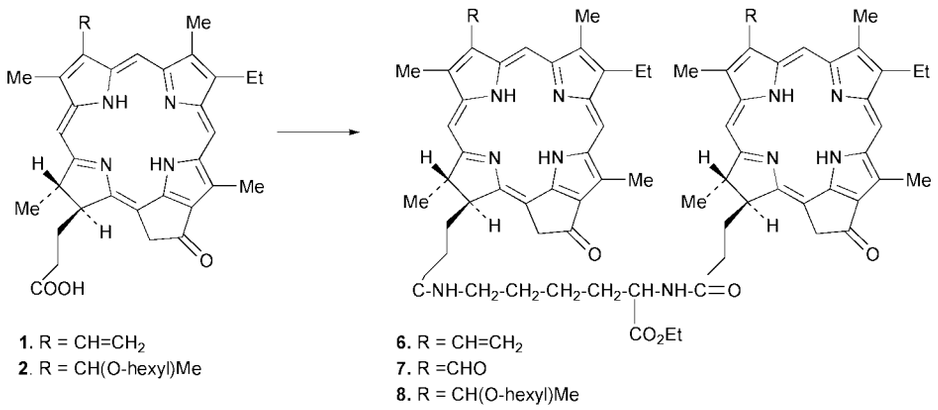

1. R = CH=CH_2
2. R = CH(O-hexyl)Me

6. R = CH=CH_2
7. R =CHO
8. R = CH(O-hexyl)Me

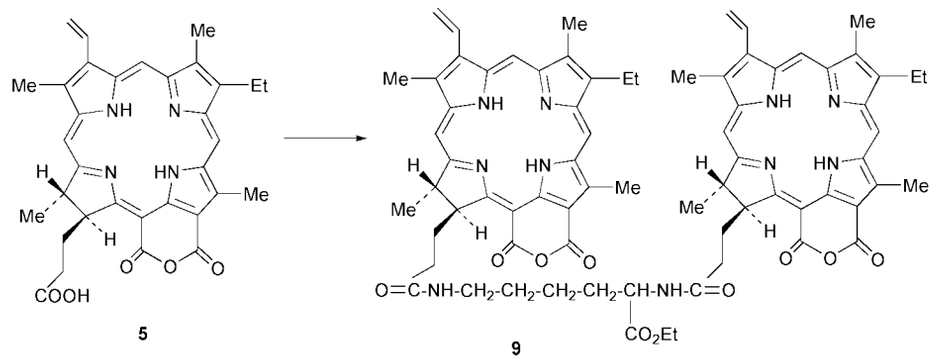

5 **9**

Scheme 1

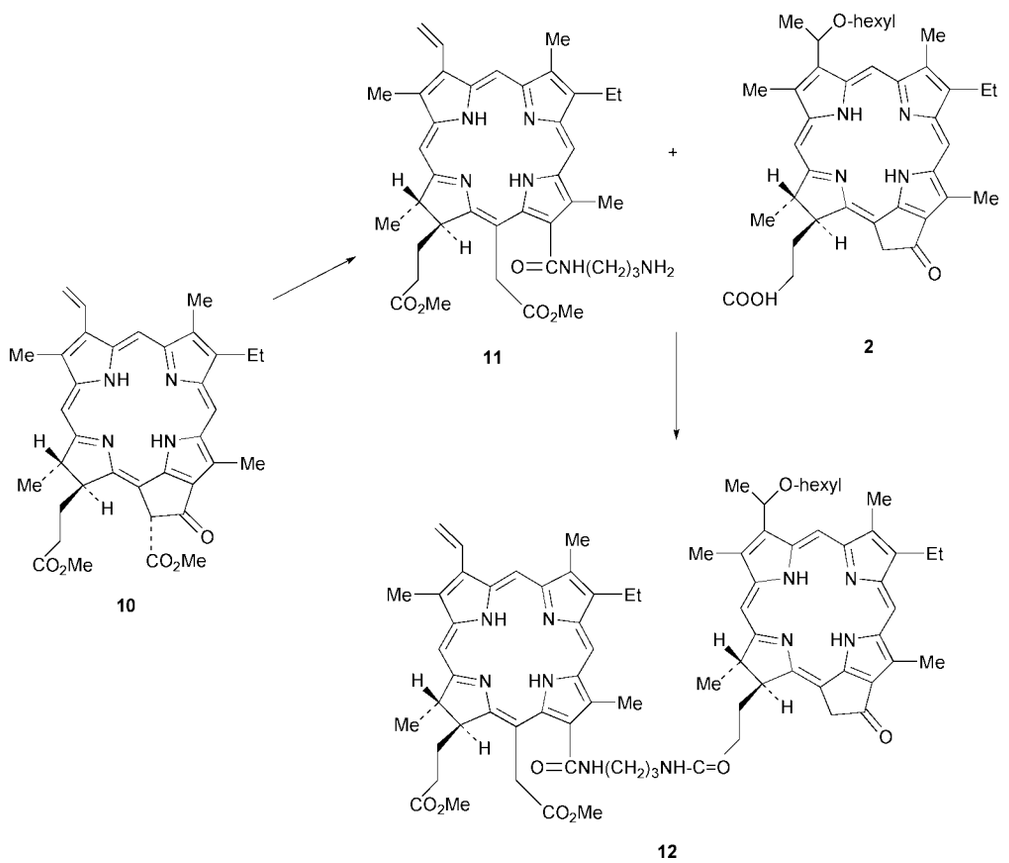

10 **11** **2** **12**

Scheme 2

tion at 698 nm (*in vivo* absorption), at a dose of 2.5 μmol kg^{-1} produced 60% tumor response on day 20; however, on day 30 tumor regrowth was observed in all mice. In purpurin 18 **5**, the fused anhydride ring tended to cleave *in vivo*, resulting in the formation of a new chromophore absorbing outside the laser window of accessibility. Therefore, due to the unstable nature of the fused anhydride ring, dimer **9** was not evaluated for *in vivo* activity.

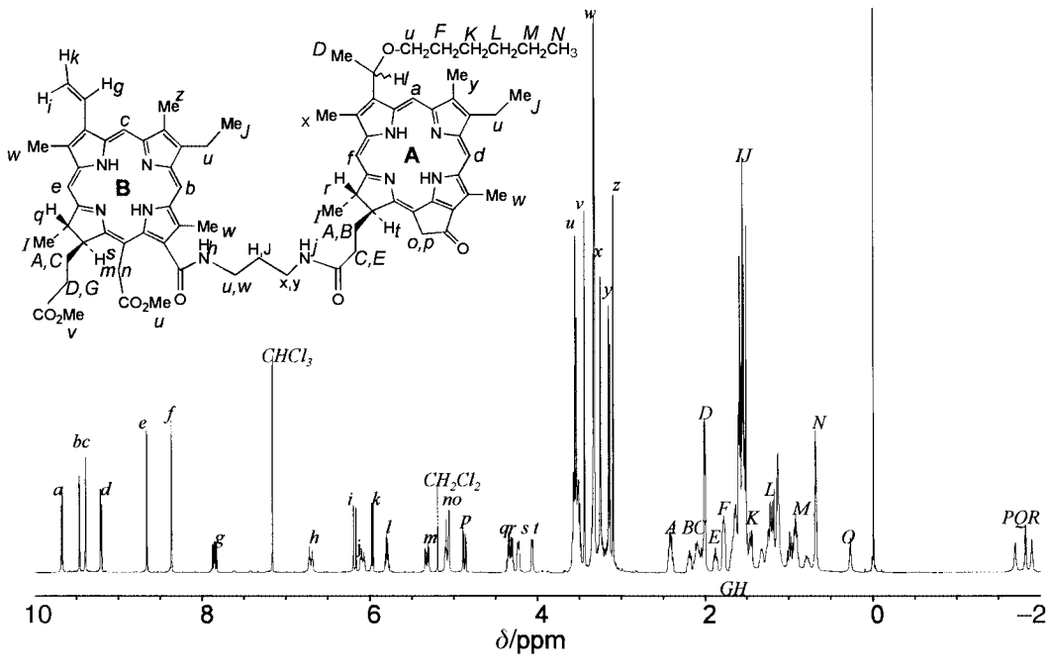

Fig. 1 ^{1}H NMR spectrum of unsymmetrical dimer **12** (in $CDCl_3$).

The symmetrical dimers **6**, **7** and unsymmetrical dimer **12** were also evaluated in mice and their results were compared with those obtained from HPPH **2**. Dimer **12** gave a partial tumor response (20% tumor cure at day 30) at a higher dose (4 μmol kg^{-1}) than for HPPH (0.4 μmol kg^{-1}) while at lower doses no antitumor activity was observed. HPPH–lysine linked dimer **8** produced some PDT efficacy (50% response at day 7 at 1.0 μmol kg^{-1}). However, at day 30, tumor regrowth was observed. Compared with the formylchlorin **3**, which showed significant PDT efficacy (60% tumor control at day 7 at 2.5 mg kg^{-1} 24 h post injection of the drug), the corresponding dimer **7** did not show any tumor necrosis (data not included in Table 1). Therefore, in contrast to the results reported by Ando *et al.*,[10] the dimers with amide linkages showed limited PDT efficacy. The conversion of a very active monomeric photosensitizer (*e.g.*, HPPH) into symmetrical and unsymmetrical dimers with amide linkages only led to a significant decrease in its antitumor activity in spite of relatively high singlet oxygen yields (see Table 4, below). These results are also in contrast to those obtained from porphyrin-based dimers with ether and carbon–carbon linkages joined at position 3 or at position 8 of the macrocycles. Therefore, the reasons for lack of efficacy of these compounds might be either due to the site(s) of the linkers joining the two molecules (which is certainly different than those effective ether- and carbon–carbon-linked dimers), or the severe aggregation caused by the presence of two hexyl ether side-chains. In order to understand the importance of localization of the drugs in cells, cellular and subcellular localization studies are currently in progress.

Photophysical properties

For a compound to be effective as a diagnostic and therapeutic agent, it is necessary for it to have the ability to produce high fluorescence (to aid in detection) and singlet oxygen yields (for effective photodynamic action) respectively. Thus, the newly synthesized dimers were evaluated for detailed photophysical properties.

Fluorescence studies

A typical fluorescence spectrum of dimer **6** along with that of H_2TPP are shown in Fig. 2. Fluorescence quantum yields and fluorescence emission maxima of these dimers are reported in Table 3. As can be seen in Table 3, compounds **8** and **12** have a similar fluorescence quantum yield ($\Phi_f \approx 0.36$) whereas compound **6** is characterized by a rather lower fluorescence yield (Φ_f 0.144). Significantly lower fluorescence yields were displayed by dimers **7** and **9**.

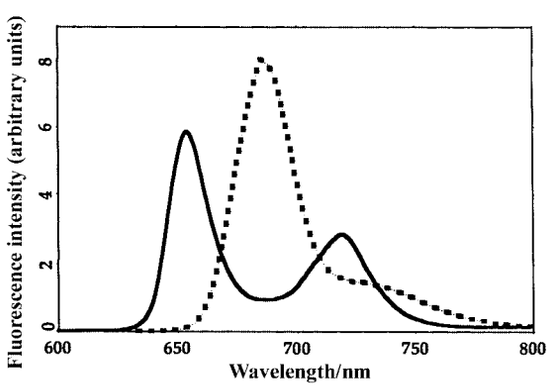

Fig. 2 Fluorescence spectra of air-saturated solutions of H_2TPP (▬) and **6** (■ ■ ■) in benzene. Optical absorptions were matched (0.06) at the excitation wavelength λ_{exc} = 410 nm.

Transient absorption studies

The transient absorption spectra of all the dimers were measured at 0.45 μs after a 6 ns pulse of 355 nm radiation incident upon an argon-saturated solution in benzene. The negative absorption at 360 nm and 700 nm for compound **6** was due to bleaching of the ground-state absorption peaks. The positive absorption near 320 nm and 460 is reminiscent of similar maxima in $T_1 \longrightarrow T_n$ spectra reported in previous investigations from our laboratories.[8] At low laser intensity, the 460 nm absorption decayed exponentially with a lifetime of 230 μs. Experiments with other compounds showed similar spectral features. However, compounds **12** and **8** exhibited triplet lifetimes of 464 μs and 384 μs respectively, significantly longer than those of the other compounds.

Triplet state quenching by oxygen

For all compounds, under air-saturated conditions in benzene, the decay of the triplet state (T_1) was enhanced over that in

Table 1 ^{1}H NMR assignments of HPPH–isochlorin e_4 linked dimer **12**

Code	Chemical shift (δ)	Integration (signal type)	Assignments	NOEs with	Couplings with
a	9.68	1 (s, splitting)	5-H(A[a])	y, l	
b	9.47	1 (s)	10-H(B[b])	w, u	
c	9.40	1 (s)	5-H(B)	z, g	
d	9.21	1 (s, splitting)	10-H(A)	u, w	
e	8.66	1 (s)	20-H(B)	w, I, q	
f	8.37	1 (s)	20-H(A)	r, t, x, I	
g	7.86	1 (dd)	3^1-H(B)	c, i, k, w	i, k
h	6.70	1 (dd, splitting)	NH		u, w, H, J
i	6.18	1 (d)	*E*-3^2-H(B)	g, k, w	g, k
j	6.09	1 (dd, splitting)	NH		x, y, H, J
k	5.97	1 (d)	*Z*-3^2-H(B)	g, i	g, i
l	5.80	1 (m)	3^1-H(A)	a, u, x, D	D
m	5.32	1 (dd)	15^1-H(B)	n, s	
n	5.09	1 (dd)	15^1-H(B)	m	
o	5.08	1 (d)	15^1-H(A)	p, A	
p	4.88	1 (dd)	15^1-H(A)	o, t	
q	4.35	1 (q)	18-H(B)	e, A, D, I	I
r	4.31	1 (q)	18-H(A)	f, A, B, C, E, I	I
s	4.23	1 (m)	17-H(B)	m, A, C, D, I	A
t	4.07	1 (d)	17-H(A)	f, p, A, B, C, E, I	A
u	3.55	10 (m)	15^2-CO_2CH_3 3^1-OC$H_2$$CH_2CH_2CH_2CH_2CH_3$ 8-C$H_2$$CH_3$(A), 8-C$H_2$$CH_3$(B) 1 × NHC$H_2$$CH_2CH_2NH$	d, b, l, H	
v	3.44	3 (s, splitting)	17^3-CO_2CH_3		
w	3.33	10 (m)	2-CH_3(B), 12-CH_3(B), 12-CH_3(A) 1 × NHC$H_2$$CH_2CH_2NH$	b, d, e, g, i, H	
x	3.25	4 (m)	2-CH_3(A) 1 × $NHCH_2CH_2C$$H_2$NH	f, l, D	
y	3.15	4 (m)	7-CH_3(A) 1 × $NHCH_2CH_2C$$H_2$NH	a, J	
z	3.10	3 (s)	7-CH_3(B)	c, J	
A	2.42	2 (m)	1 × 17^1-H(B), 1 × 17^1-H(A)	o, q, r, s, t, C, D	s, t
B	2.19	1 (m)	1 × 17^1-H(A)	r, t, E	
C	2.10	2 (m)	1 × 17^1-H(B), 1 × 17^2-H(A)	r, s, t, A, D	
D	2.01	4 (m)	3^1-CH_3(A), 1 × 17^2-H(B)	l, q, l, x, C, G	l
E	1.88	1 (m)	1 × 17^2-H(A)	r, t, B	
F	1.78	2 (m)	3^1-$OCH_2C$$H_2$$CH_2CH_2CH_2CH_3$	M	M
G	1.68	1 (m)	1 × 17^2-H(B)	D	
H	1.64	1 (m)	1 × $NHCH_2C$$H_2$$CH_2NH$	u	s, t
I	1.59	6 (m)	18-CH_3(A), 18-CH_3(B)	e, f, q, r, s, t	q, r
J	1.55	7 (m)	8-$CH_2C$$H_3$(A), 8-$CH_2C$$H_3$(B) 1 × $NHCH_2C$$H_2$$CH_2NH$	z, y	
K	1.46	2 (m)	3^1-$OCH_2CH_2C$$H_2$$CH_2CH_2CH_3$	M	
L	1.13	2 (m)	3^1-$OCH_2CH_2CH_2C$$H_2$$CH_2CH_3$	N	N
M	0.92	2 (m)	3^1-$OCH_2CH_2CH_2CH_2C$$H_2$$CH_3$	F, K, N	F
N	0.69	3 (m)	3^1-$OCH_2CH_2CH_2CH_2CH_2C$$H_3$	L, M	L
O	0.27	1 (br s)	ring NH		
P	−1.70	1 (br s)	ring NH		
Q	−1.82	1 (br s, splitting)	ring NH		
R	−1.90	1 (br s)	ring NH		

[a] Macrocycle A = pyropheophorbide *a*. [b] Macrocycle B = isochlorin e_4.

deaerated solutions. This decay was exponential and resulted in the formation of singlet oxygen (see below). The variation of the observed rate constant k_o was measured at different oxygen concentrations by bubbling O_2–Ar mixtures of known composition through the solutions. For all compounds, a linear variation was observed. From the slopes of these linear variations, bimolecular rate constants $k_{T\Sigma}$ for energy transfer from the T_1 triplet state to O_2 ground state ($^3\Sigma_g^-$) were extracted and reported in Table 4. For all dimers, this energy-transfer process (the quenching of the triplet state T_1 by ground-state O_2) is governed by a similar bimolecular rate constant $k_{T\Sigma}$ of the order of 2×10^9 M^{-1} s^{-1}, a value which is in the realm of diffusion-limited rate constants.

Singlet oxygen quantum yield ($^1\Phi_\Delta$)

Singlet oxygen quantum yields were determined by monitoring the decay kinetics of the near-IR (NIR) luminescence intensity resulting from photoexcitation at 355 nm. All samples displayed NIR luminescence showing a prompt increase in intensity that decayed back to the initial baseline. As outlined in the Experimental section, the slow component is the emission from singlet oxygen formed by energy transfer from the photosensitizer to ground-state molecular oxygen. To separate the decay profile of singlet oxygen from that of the fast component, the start of the fitting routine was delayed until consistent values for $\tau_\Delta = 33$ μs were obtained, typical of O_2 ($^1\Delta_g$) in benzene.[13,14] Under these conditions the evaluated L_o-values are accurate representations of Φ_Δ. For a given compound L_o-values were plotted as a function of laser energy. The slopes of the early linear regions of such plots, compared to that of the selected reference material (see Experimental section), allowed singlet oxygen quantum yields to be derived. These are reported in Table 4. As it can be seen from this Table, high singlet oxygen quantum yields ($\Phi_\Delta \approx 0.50$) were obtained for compounds **8** and **12**, making them effective therapeutic agents in PDT.

Table 2 Comparative *in vivo* photosensitizing activity[a]

Compounds	Absorbance *in vivo* (nm)	Dose: 0.4 μmol kg^{-1} Tumor response (%) [days]			Dose: 1.0 μmol kg^{-1} Tumor response (%) [days]			Dose: 4.0 μmol kg^{-1} Tumor response (%) [days]		
		2	7	30	2	7	30	2	7	30
Pyropheophorbide[a] **1**	665	0	0	0	0	0	0	All mice died post light treatment		
3-Devinyl-3-formylpyropheophorbide[a] **3**	698	0	0	0	0	0	0	All mice died post light treatment		
Pyropheophorbide[a] hexyl ether (HPPH) **2**	665	100	100	60	100	100	100	Not determined		
Chlorin e_6 trimethyl ester **4**	665	0	0	0	0	0	0	All mice died post light treatment		
Purpurin 18 **5**	699	Not stable *in vivo*								
Purpurin 18–lysine linked dimer **9**	699	Not stable *in vivo*								
Pyropheophorbide–lysine linked dimer **6**	665	0	0	0	0	0	0	All mice died post light treatment		
3-Devinyl-3-formylpyropheophorbide *a*–lysine linked dimer **7**	698	0	0	0	0	0	0	All mice died post light treatment		
HPPH–lysine linked dimer **8**	665	0	0	0	100	50	0	All mice died post light treatment		
HPPH–chlorin e_6-linked dimer **12**	665	0	0	0	0	0	0	100	100	20

[a] Groups of DBA-2 mice (6 mice) bearing 4–6 diameter RIF tumor were exposed to 75 mW cm^{-2} for 30 min to deliver 135 J cm^{-2} from a tunable dye laser tuned to the maximum red absorption peak determined by *in vivo* reflectance spectroscopy. Time between injection and light treatment was 24 h.

Table 3 Absorption maxima (Q-band), fluorescence emission maxima and fluorescence quantum yields (Φ_f)

Compound	λ_{max} (absorption)/nm	λ_{max} (emission)/nm	Φ_f
6	675	693	0.144
7	700	722	0.067
8	663	676	0.37
9	706	717	0.005
12	664	669	0.36

Table 4 Triplet-state parameters (defined in text) and singlet oxygen quantum yields (Φ_Δ)

Compound	$10^{-3}k_o$/s^{-1} (± 2%)	τ_T/μs	λ_T^{max}/nm	$10^{-9}k_{T\Sigma}$/ M^{-1} s^{-1} (± 5%)	Φ_Δ ± 0.05
6	4.0	230	340, 460	2.61	0.36
7	5.8	172	340, 480	2.66	0.26
8	2.6	384	320, 460	2.03	0.48
9	4.2	238	320, 460	1.86	0.06
12	2.1	464	320, 440	2.20	0.49

Relatively high fluorescence quantum yields ($\Phi_f \approx 0.40$) were also observed for compounds **8** and **12**. In both cases the sum of Φ_f and Φ_Δ is close to 0.90, indicating that the intersystem crossing from the S_1 state to the T state (and consequently singlet-oxygen production) and fluorescence account for ≈90% of the absorbed photons. This implies that the triplet quantum efficiency and the yield of singlet oxygen are probably comparable. Compound **9** shows a very low singlet oxygen quantum yield ($\Phi_\Delta = 0.06$). Singlet oxygen is produced *via* energy transfer from the photosensitizer triplet state to ground-state molecular oxygen. Triplet-state formation is dependent upon three different competitive processes originating in the excited singlet state. These are (i) intersystem crossing from S_1 to T, (ii) fluorescence from S_1 to S_0, and (iii) intersystem crossing from T to S_0. The intrinsic lifetime of the T_1 state (Table 3) is similar to that of other compounds studied, as is the rate constant for oxygen quenching. The very low fluorescence quantum yield ($\Phi_f = 0.005$) observed with this compound supports this conclusion as it is indicative that the major deactivation channel of S_1 is rapid conversion to the ground-state surface. This would result in a diminished triplet quantum yield, and hence a low yield of singlet oxygen.

The two other compounds of this series (compounds **6** and **7**) have singlet oxygen quantum yields in the range 0.26–36. Thus, these dimers with amide linkages have triplet states with energies relatively higher than that of singlet oxygen such that irreversible exchange energy transfer is always observed. In this they resemble the alkyl ether analogs of chlorophyll *a* derivatives and some other novel bacteriochlorins that have been synthesized and photophysically characterized in our laboratories.[8]

Conclusions

This work deals with the synthesis, *in vivo* biological activity, singlet oxygen and fluorescence quantum yields of a series of long-wavelength-absorbing (λ_{max} 660–702 nm) chlorin-based symmetrical and unsymmetrical dimers with amide linkages. All compounds demonstrated that efficient energy transfer from the sensitizer triplet to ground state of molecular oxygen is irreversible ($k_{T\Sigma} \approx 2 \times 10^9$ M^{-1} s^{-1}), an indication that their triplet state energies are relatively higher than that of singlet oxygen. High fluorescence ($\Phi_f \approx 0.35$) and singlet oxygen quantum yields (≈0.50) were generated from compounds **8** and **12** of the series. For these two compounds, the sum of Φ_f and $\Phi_\Delta \approx 0.90$, indicating that S_1–T intersystem crossing and fluorescence accounts for ≈90% of the absorbed photons. Although compounds **6** and **7** generated less singlet oxygen yield than compounds **8** and **12**, their singlet oxygen quantum yields are in the range 0.26–0.36. Compound **9** showed a very low fluorescence and low singlet oxygen yields. This lack of singlet oxygen production may be related to a highly efficient S_1–S_0 internal conversion, which diminishes the triplet quantum yield (and hence singlet oxygen production).

Experimental

Solvents were purified according to the guidelines in ref. 15. Mps are uncorrected and were measured by hot-plate apparatus. NMR spectra were recorded in a Bruker 400 MHz instrument. Mass spectrometry analyses were carried out at the Mass Spectrometry Facility, Department of Biochemistry, Michigan State University, East Lansing and the Department of Molecular and Cellular Biophysics, Roswell Park Cancer

Institute, Buffalo. Elemental analyses were carried out at the Midwest Microlab, LLC, Indianapolis, Indiana.

3-Devinyl-3-(1′-hexyloxyethyl)pyropheophorbide *a* (HPPH) 2

Pyropheophorbide *a* (100 mg) was treated with 30% HBr–acetic acid (2.5 mL) at room temperature. The acids were removed under high vacuum at low temperature (< 40 °C) for 2 h. The unstable intermediate bromo analog was not isolated and was immediately treated with hexan-1-ol (1.5 mL) in dry dichloromethane (10 mL) containing anhydrous potassium carbonate (200 mg) for 45 min at room temperature. The reaction mixture was diluted with dichloromethane. The organic layer was separated, washed with water, and dried over anhydrous sodium sulfate. Evaporation of the solvent gave a residue, which was chromatographed over an alumina column (grade III) with CH_2Cl_2 as eluent. The major band was collected. Evaporation of the solvent gave the title compound as a sticky solid (90 mg, 80%). ^{1}H NMR (400 MHz; 3 mg mL^{-1} $CDCl_3$; δ ppm) 9.77, 9.52 and 8.51 (each s, 1H, 5-, 10- and 20-H), 5.89 (q, 1H, 3^1-H), 5.20 (ABX, 2H, 13^2-CO_2CH_3), 4.41 (m, 1H, 18-H), 4.28 (m, 1H, 17-H), 3.70 (q, 2H, 8-CH_2CH$_3$), 3.68, 3.60, 3.37 and 3.26 (each s, 3H, for 3 × ring CH_3 and 17^3-CO_2CH_3), 2.70, 2.56 and 2.30 (each m, total 4H, for 2 × 17^1-H and 2 × 17^2-H), 2.10 (d, 3H, 3^2-CH_3), 1.82 (d, 3H, 18-CH_3), 1.70 (d, 3H, 8-CH_2CH_3), 1.31–0.76 (several m, total 13H, OCH_2CH_2-$CH_2CH_2CH_2CH_3$), 0.43 and −1.71 (each br s, 1H, 2 × NH). Reaction of the methyl ester analog with aq. LiOH produced the carboxylic derivative **2**. The NMR spectrum of **2** was similar to the corresponding methyl ester, except the peak at 3.68 ppm was missing. HRMS Calc. for $C_{40}H_{50}N_4O_4$: *m*/*z*, 650.3826. Found: *m*/*z*, 650.3820.

13^1-[3′-Aminopropylcarbamoyl]isochlorin e_4 dimethyl ester 11

Pheophorbide *a* methyl ester **10** (430 mg) was dissolved in chloroform (50 mL) and 1,3-diaminopropane (1.8 mL) was added. The reaction mixture was refluxed under nitrogen for 24 h. After evaporation of the solvent, the residue was chromatographed on an alumina column (eluted first with dichloromethane to remove the unchanged **10**, then switched to 10% MeOH–dichloromethane to collect the product). After crystallization from dichloromethane–hexanes, the title compound was obtained (380 mg, 79%). ^{1}H NMR (400 MHz; 3 mg mL^{-1} $CDCl_3$; δ ppm) 9.67, 9.62 and 8.80 (each s, 1H, 5-, 10- and 20-H), 8.05 (dd, 1H, 3^1-C*H*=CH_2), 7.11 (br s, 1H, CON*H*CH_2-$CH_2CH_2NH_2$), 6.33 (d, 1H, *E*-3^2-CH=C*H*H), 6.09 (d, 1H, *Z*-3^2-CH=C*H*H), 5.38 (ABX, 2H, 15-CH_2), 4.44 (q, 1H, 18-H), 4.37 (d, 1H, 17-H), 3.78 (s, 3H, 15-$CH_2CO_2CH_3$), 3.76 (m, 2, 8^1-CH_2), 3.61 (s, 3H, 12-CH_3), 3.52 (s, 3H, 17^3-CO_2CH_3), 3.48 and 3.29 (each s, 3H, 2- and 7-CH_3), 2.92 (m, 2H, $CONHCH_2$-$CH_2CH_2NH_2$), 2.56 and 2.17 (each m, 1H, for 2 × 17^1-H and 2 × 17^2-H), 1.84 (m, 6H, $CONHCH_2CH_2CH_2NH_2$), 1.70 (d and t, 6H, 18- and 8^2-CH_3), −1.61 and −1.84 (each br s, 1H, 2 × NH); UV/vis [λ_{max}/nm (ε/dm^3 mol^{-1} cm^{-1}) in CH_2Cl_2] 402 (115 900), 500 (10 900), 528 (3500), 560 (1800), 608 (4100), 662 (36 700); mp >300 °C; mass (HRMS): Calc. for $C_{39}H_{48}N_6O_5$: *M*, 680.3686. Found: M^+, 680.3673. Analysis: Calc. for $C_{39}H_{48}N_6O_5 \cdot 2H_2O$: C, 65.33; H, 7.32; N, 11.73. Found: C, 65.88; H, 6.81; N, 11.21%.

The pyropheophorbide *a* linked dimer 6

Pyropheophorbide *a* **1** (100 mg) was dissolved in dichloromethane (40 mL) along with DCC (150 mg), L-lysine (12 mg) and DMAP (10 mg). The reaction mixture was stirred at room temperature for 24 h. After regular work-up and purification, the title compound was obtained (63 mg, 70% yield on the basis of L-lysine). ^{1}H NMR (400 MHz; 3 mg mL^{-1} $CDCl_3$; δ ppm) 9.20, 8.95, 8.20 and 8.02 (each s, 1H, 4 × *meso* H), 8.38 (s, 2H, 2 × *meso* H), 7.85, 7.60 (each dd, 1H, 2 × 3^1-C*H*=CH_2), 7.05 and 6.95 (d, and br, 1H, 2 × CONH), 5.90–6.25 (m, 4H, 2 × CH=CH_2), 5.12–3.87 [eight m, total 11H, C*H*(CO_2CH_3), 2 × 17-H, 2 × 18-H, $CO_2CH_2CH_3$, 2 × 13^2-CH_2], 3.30, 3.20, 3.18 and 3.00 (each s, 3H, 4 × CH_3), 2.10 (s, 6H, 2 × CH_3), 3.42 and 3.20 (each q, 2H, 2 × CH_2CH$_3$), 2.18 and 2.40 (each m, 4H, 2 × 17^1-H and 2 × 17^2-H), 1.62 [(two d merged), 6H, 2 × 18-CH_3], 1.20–1.50 [m, 8H, $(CH_2)_4$], 1.41, 1.29 and 1.24 (each t, 3H, 2 × 8-CH_2CH_3 and $CO_2CH_2CH_3$), 0.88, 0.16, −1.65 and −1.75 (each br s, 1H, 4 × NH); UV/vis [λ_{max}/nm (ε/dm^3 mol^{-1} cm^{-1}) in CH_2Cl_2] 377 (118 300), 400 (162 000), 412 (159 100), 510 (18 200), 540 (15 400), 420 (15 000), 668 (71 500); LRMS: Calc. for $C_{74}H_{82}N_{10}O_6$: *M*, 1206.6418. Found: M^+, 1207.3 Analysis: Calc. for $C_{74}H_{82}N_{10}O_6 \cdot H_2O$: C, 72.51; H, 6.91; N, 11.43. Found: C, 72.88; H, 7.00; N, 11.29%.

The 3,3′-didevinyl-3,3′-diformylpyropheophorbide *a* linked dimer 7

Pyropheophorbide *a* methyl ester (400 mg) was dissolved in THF (200 mL). OsO_4 (120 mg) in CCl_4 (20 mL) and sodium periodate (2.8 g) in water (120 mL) were added. This reaction mixture was stirred at room temperature under nitrogen for 4 h, and was monitored by UV-visible spectrophotometry (disappearance of the peak at 666 nm, and appearance of a new peak at 693 nm). It was then diluted with dichloromethane (200 mL), and washed successively with 2% aq. acetic acid and water. The organic layer was separated, and dried over anhydrous sodium sulfate. Evaporation of the solvent gave a residue, which was chromatographed over an alumina column (grade III) and eluted with dichloromethane. The major band was collected. Solvent was removed and the 3-formylpyropheophorbide methyl ester was crystallized from dichloromethane–hexane in 66% (265 mg) yield, mp 190–193 °C. It was then converted into carboxylic acid **3** by reaction with LiOH–methanol–THF in quantitative yield. Further reaction of **3** with L-lysine–DCC and DMAP under the reaction conditions discussed for dimer **6** produced the title compound **7** in 60% yield, mp >300 °C; ^{1}H NMR (400 MHz; 3 mg mL^{-1} $CDCl_3$; δ ppm) 11.27 and 11.05 (each s, 1H, 2 × 3-CHO), 10.03, 9.77, 8.50 and 8.34 (each s, 1H, 4 × *meso*-H), 8.53 (s, 2H, 2 × *meso*-H), 6.92 and 6.76 (d, and br, 1H, 2 × CONH), 5.14–3.92 [eight m, total 13H, 1 × $CH(CO_2C_2H_5)$, 2 × 17-H, 2 × 18-H, 2 × $CO_2CH_2CH_3$, 2 × 13^2-CH_2], 3.53, 3.43, 3.25 and 3.03 (each s, 3H, 4 × CH_3), 2.49 (s, 6H, 2 × CH_3), 3.47 and 3.19 (each m, 2H, 2 × CH_2CH$_3$), 2.46 and 2.30 (each m, 4H, 2 × 17^1-H and 17^2-H), 1.66 (two d merged, 6H, 2 × 18-CH_3), 1.20–1.50 [m, 4H, $(CH_2)_4$], 1.45, 1.34 and 1.24 (each t, 3H, 2 × 8-CH_2CH_3 and $CO_2CH_2CH_3$), 0.90, −0.55, −1.60 and −1.80 (each br s, 1H, 4 × NH); UV/vis [λ_{max}/nm (ε/dm^3 mol^{-1} cm^{-1}) in CH_2Cl_2] 389 (110 500), 418 (102 000), 522 (14 300), 556 (14 800), 694 (70 700); Mass (FAB): Calc. for $C_{72}H_{78}N_{10}O_8$: *M*, 1210.6. Found: 1211.6 (M + 1). Analysis: Calc. for $C_{72}H_{78}N_{10}O_8 \cdot H_2O$: C, 70.32; H, 6.56; N, 11.40. Found: C, 70.42; H, 6.92; N, 11.13%.

HPPH–lysine linked dimer 8

HPPH **2** (110 mg) was dissolved in dichloromethane (40 mL) along with DCC (150 mg), L-lysine (12 mg) and DMAP (10 mg). The reaction mixture was stirred at room temperature for 24 h. After the regular work-up and purification, the title compound was obtained (65 mg, 62%); mp, turned sticky at 150 °C; ^{1}H NMR (400 MHz; 3 mg mL^{-1} $CDCl_3$–pyridine-d_5 (5 μL); δ ppm) due to the presence of multiple asymmetrical centers, the NMR spectrum is complex; however, tentative resonance assignments are given as follows: 9.75, 9.73, 9.71 and 9.69 (each s, $\frac{1}{2}$H, for 2 × *meso*-H), 8.48, 8.47 and 8.46 (each s, total 2 × *meso*-H), 8.25 (br s, 1H, *meso*-H), 8.08 and 8.03 (each br s, $\frac{1}{2}$ H, 1 × *meso*-H), 7.69 and 6.94 (each m, 1H for 2 × 3^1-H), 7.14 (m, 2H, 2 × CONH), 5.90 (two q, each 1H, for 2 × 18-H), 5.26–4.65 (two ABX, each 2H, for 2 × 13^2-CH_2), 4.60, 4.48,

4.23 and 4.14 (each m, total 5H, 2 × 17-H, CONHC*H*-$CO_2C_2H_5$, $CO_2CH_2CH_3$), 3.66 (m, 4H, 2 × 8-CH_2CH_3), 3.37, 3.36, 3.35 and 3.34 (each s, total 6H, 2 × CH_3), 3.26, 3.25, 3.24, 3.23, 3.15 and 3.18 (each s, total 6H, for 2 × CH_3), 2.49 [m, total 8H, for 2 × (2 × 17^1-H and 2 × 17^2-H)], 2.18–2.06 (m, 12H, 2 × ring CH_3 and 2 × 18-CH_3), ≈1.71 and 1.56–1.18 (m, 3H, 2 × 3^2-CH_3, CONHCHCH_2CH_2CH_2CH_2NHCO, OCH_2CH_2-CH_2CH_2CH_2CH_3 and $CO_2CH_2CH_3$), 0.83 and 0.76 (each m, 3H, 2 × $OCH_2CH_2CH_2CH_2CH_2CH_3$), −1.47 and −1.55 (each br s, 2H, 2 × 2NH); UV/vis [λ_{max}/nm (ε/dm^3 mol^{-1} cm^{-1}) in CH_2Cl_2] 660 (55 000), 537 (12 400), 507 (12 700) and 408 (124 000). Analysis: Calc. for $C_{86}H_{110}N_{10}O_8$: C, 73.15; H, 7.86; N, 9.93. Found: C, 73.35; H, 7.66; N, 9.90%.

The purpurin 18 linked dimer 9

Purpurin 18 **5** (100 mg) was dissolved in dichloromethane (40 mL) along with DCC (150 mg), L-lysine (12 mg) and DMAP (10 mg). The reaction mixture was stirred at room temperature for 24 h. After the regular work-up and purification, the title compound was obtained (76 mg, 72% yield on the basis of L-lysine); ^{1}H NMR (400 MHz; 3 mg mL^{-1} $CDCl_3$; δ ppm) 9.08, 8.95, 8.93, 8.93, 8.41 and 8.40 (each s, 1H, 6 × *meso* H), 7.55–7.74 (m, 2H, 2 × C*H*=CH_2), 6.82 and 6.70 (d and t, 1H, CONH), 6.01–6.20 (m, 4H, 2 × CH=CH_2), 4.31 and 4.88 (each m, 2H, 2 × 17-H and 18-H), 4.60 [m, 1H, C*H*(CO_2-C_2H_5)], 4.13 (q, 2H, $CO_2CH_2CH_3$), 3.41 and 3.22 (q, 2H, 2 × C$H_2$$CH_3$), 3.21, 3.18, 3.15, 3.04, 2.99 and 2.86 (each s, 3H, 6 × CH_3), 2.19–2.55 (each m, 2H, 2 × 17^1-H and 2 × 17^2-H), 1.84 [(s and d merged), 6H, 2 × 8-CH_3], 1.49–1.59 [m, 8H, $(CH_2)_4$], 1.22–1.26 (m, 6H, 2 × CH_2CH_3), 0.88 (t, 2H, CO_2CH_2-CH_3), −0.39 and −0..43 (each s, H, 2 × NH), −0.48 (s, 2H, 2 × NH); UV/vis [λ_{max}/nm (ε/dm^3 mol^{-1} cm^{-1}) in CH_2Cl_2] 408 (174 200), 482 (8200), 510 (11 000), 548 (36 000), 594 (5500), 650 (16 500), 702 (21 800); mp > 300 °C; Mass (FAB) Calc. for $C_{74}H_{78}N_{10}O_{10}$: *M*, 1266.5. Found: 1267.2 (M + 1). Analysis: Calc. for $C_{74}H_{78}N_{10}O_{10}$: C, 70.11; H, 6.21; N, 11.06. Found: C, 69.87; H, 6.34; N, 10.82%.

Unsymmetrical linked dimer 12

Chlorin e_6 13^1-[(3′-aminopropyl)amide] dimethyl ester **11** (52 mg) and HPPH **2** (50 mg) were dissolved in dichloromethane (50 mL). DCC (150 mg) and DMAP (10 mg) were added. By following a method similar to that for the preparation of pyropheophorbide *a* dimer **6**, the title compound was obtained (72 mg, 70%); ^{1}H NMR (600 MHz; 5 mg mL^{-1} $CDCl_3$; δ ppm) assignments of all protons are summarized Table 1; ^{13}C NMR (400 MHz; 10 mg mL^{-1} $CDCl_3$; δ ppm; chemical shifts are reported relative to $CDCl_3$ at δ_C 77) 196.13, 173.70, 173.45, 172.67, 171.64, 169.90, 168.82, 166.65, 160.38, 155.16, 150.73, 148.93, 144.88, 144.70, 141.35, 139.67, 138.92, 137.63, 136.14, 135.98, 135.56, 134.97, 134.84, 134.55, 132.19, 130.28, 130.15, 129.79, 129.37, 127.91, 121.50, 105.94, 103.90, 102.11, 101.40, 98.73, 97.93, 97.85, 93.58, 92.53, 72.82, 69.69, 53.10, 52.04, 51.69, 51.49, 49.98, 49.13, 47.98, 37.97, 37.26, 36.29, 33.90, 32.98, 31.71, 31.08, 30.20, 29.62, 26.08, 25.62, 24.93, 24.66, 22.96, 22.54, 19.58, 19.43, 17.58, 17.35, 13.93, 12.05, 11.97, 11.82, 11.28, 11.20, 10.97, 1.01, −0.03 (total 78 peaks, the *R*/*S* isomeric nature of dimer **12** due to the hexyl ether functionality was not distinguishable in the ^{13}C spectrum); UV/vis [λ_{max}/nm (ε/dm^3 mol^{-1} cm^{-1}) in CH_2Cl_2] 404 (221 300), 502 (20 500), 534 (10 800), 606 (10 000), 660 (90 000); mp >300 °C (decomposes at 260 °C); Mass: Calc. for $C_{79}H_{95}N_{10}O_8$: 1299.7 (*M*). Found: M^+, 1299.8. Analysis: Calc. for $C_{78}H_{95}N_{10}O_8 \cdot H_2O$: C, 71.03; H, 7.42; N, 10.83. Found: C, 71.14; H, 7.91; N, 10.63%.

Photophysical studies

Laser flash photolysis. Nanosecond laser flash photolysis experiments were performed using the third harmonic (355 nm) of a continuum Surelite I Q-switched Nd:YAG laser that generates pulses of 6 ns duration. The solutions were contained in a 1 × 1 cm cuvette and the generated transient species were monitored at right angles to the laser beam. The solutions were continuously stirred with a stream of the purging gas except where aerated systems were employed. Kinetic analyses were carried out using a computer-controlled kinetic spectrometer described elsewhere.[16] Kinetic data were obtained from the averaging of 10 individual laser shots. The point-by-point differential spectra of the different compounds were obtained from the average of two individual shots at each wavelength.

Singlet oxygen luminescence. The same laser instrument described above was used to generate singlet oxygen in a 1 × 1 cm cuvette. Singlet oxygen luminescence was detected at right angles with respect to the laser beam by a germanium photodiode (Applied Detector Corp. 403HS) cooled to 77 K. A 5 mm thick silicon metal filter (AR-coated, II-VI Inc) and a 1270 nm interference filter were positioned between the sample cuvette and the photodiode detector. This combination minimized scattered light and fluorescence. The voltage output from the detector-amplifier combination was applied to the 1 MΩ input connector of a Lecroy 9450 digital CRO. Typically, 100 laser shots were averaged together at each of a series of different laser intensities selected by rotary polarizer attenuator calibrated with a power meter. The time profiles of singlet oxygen luminescence (1.27 μm) observed from such experiments are usually a composite of a fast component resulting from residual scattered laser light and near-infrared fluorescence processed through the time constant of the detector system (*ca.* 600 ns) and a slower component that arises from the singlet oxygen luminescence decay. Fitting the slow component with an exponential and extrapolating back to time 0 provides a measure of the O_2 ($^1\Delta_g$) concentration prior to the onset of the decay (L_0). Measurements of L_0 were made at a series of laser intensities for both the test solutions and for a solution of *meso*-tetraphenylporphine (H_2TPP) in benzene ($\Phi_\Delta = 0.62$)[17] having the same absorbance at 355 nm. These provided values for L_0(x) and L_0(r) for the series of laser intensities, where x and r refer to the test solution and the reference solution, respectively. At low laser intensities, the plots of L_0(x) *versus* L_0(r) were linear. From these plots, the slopes $k_{x\text{-}r}$ were extracted and used to calculate the quantum yield of singlet oxygen of the unknown solution under the prevailing conditions, according to equation (1) where *A* is

$$k_{x\text{-}r} = (\Phi^x{}_\Delta \eta^x A^x)/(\Phi^r{}_\Delta \eta^r A^r) \quad (1)$$

the absorbance at the excitation wavelength, $\Phi^x{}_\Delta$ is the singlet oxygen quantum yield ($\Phi^r{}_\Delta = 0.62$) and η is the quenching efficiency given by equation (2) where k_o is the decay rate constant of the triplet in argon-saturated solutions and $k_{T\Sigma}$ is the

$$\eta = k_{T\Sigma}[O_2]/(k_o + k_{T\Sigma}[O_2]) \quad (2)$$

bimolecular rate constant for quenching of the triplet state by oxygen. In our experiments, all measurements showed that $k_{T\Sigma} \gg k_o$, making the quotient η^x/η^r close to unity. Thus, relation (2) becomes equation (3).

$$k_{x\text{-}r} = \Phi^x{}_\Delta A^x/\Phi^r{}_\Delta A^r \quad (3)$$

Measurements of singlet oxygen O_2 ($^1\Delta_g$) generated from the standard were made before and after the measurements done with the samples under investigation, which confirmed that instrument response remained constant.

Fluorescence measurements. Fluorescence spectra were recorded with a SPEX 1680 0.22 m double Spectrofluorimeter. Fluorescence quantum yields (Φ_f) were measured relative to

meso-tetraphenylporphine (H_2TPP) in benzene ($\Phi_f = 0.11$).[18] The working equation[19] was equation (4) where $I(\lambda)$ is the

$$\Phi_f(x) = \Phi_f(r)\{A_r(\lambda_r)A_x(\lambda_x)\}\{I(\lambda_r)I(\lambda_x)\}\{n_x^2/n_r^2\}\{D_x/D_r\} \quad (4)$$

relative intensity of the excitation light at wavelength λ, n is the average refractive index of the solution to the luminescence, D is the integrated area under the corrected emission spectrum, and $A(\lambda)$ is the absorbance of the solution at the excitation wavelength.

In our experiments, the ground state absorbance of the sample and the reference solutions were matched at the same excitation wavelength $\lambda_{exc} = 410$ nm ($A_x = A_r = 0.06$). Within the same solvent (benzene) and using optically dilute solutions, the refractive index was assumed to be invariant ($n_x = n_r$). All fluorescence spectra (reference and test solutions) were recorded under identical conditions. Under such conditions, the working equation is reduced to equation (5).

$$\Phi_f(x) = \Phi_f(r)[D_x/D_r] \quad (5)$$

Quenching by oxygen. Bubbling O_2–Ar mixtures of known compositions through the solutions varied the oxygen concentrations. Benzophenone in benzene ($k_{T\Sigma} = 2.3 \times 10^9\ M^{-1}\ s^{-1}$)[20] was used to calibrate these different O_2–Ar mixtures.

Acknowledgements

We thank the National Institutes of Health (CA 55791, HL 22252) for financial support. Partial support by the shared resources of the Roswell Park Cancer Support Grant (P30CA16056) is also acknowledged. We also appreciate the help rendered by Mr Adam Sumlin and Mr William Potter (PDT Center, RPCI, Buffalo) for the *in vivo* experiments.

References

1 (*a*) R. K. Pandey and G. Zheng, *Porphyrins as Photosensitizers in Photodynamic Therapy*, *The Porphyrin Handbook*, ed. K. M. Kadish, K. M. Smith and R. Guilard, Academic Press, San Diego, 2000; (*b*) R. K. Pandey and C. Herman, *Chem. Ind.* (*London*), 1998, 739; (*c*) R. Bonnett, *Chem. Soc. Rev.*, 1995, **24**, 19.
2 T. J. Dougherty, C. Gomer, B. W. Henderson, G. Jori, D. Kessel, M. Korbelik, J. Moan and Q. Peng, *J. Natl. Cancer Inst.*, 1998, **90**, 889.
3 M. M. Siegel, K. Tabei, R. Tsao, M. J. Pastel, R. K. Pandey, S. Berkenkamp, F. Hillenkamp and M. S. de Vries, *J. Mass Spectrom.*, 1999, **34**, 661 and references therein.
4 (*a*) S. Davis, M. Weiss, J. R. Wong, T. J. Lampidis and L. B. Chen, *J. Biol. Chem.*, 1985, **260**, 13844; (*b*) D. Dolphin, *Can. J. Chem.*, 1994, **72**, 1005; (*c*) G. Li, Y. Chen, J. R. Missert, A. Rungta, T. J. Dougherty, Z. D. Grossman and R. K. Pandey, *J. Chem. Soc., Perkin Trans. 1*, 1999, 1785.
5 (*a*) R. K. Pandey, F.-Y. Shiau, T. J. Dougherty and K. M. Smith, *Tetrahedron*, 1991, **47**, 9571; (*b*) R. K. Pandey and T. J. Dougherty, *Cancer Res.*, 1989, **49**, 2042; (*c*) C. J. Byrne, I. K. Morris and A. D. Ward, *Aust. J. Chem.*, 1990, **43**, 1889; (*d*) R. K. Pandey, F.-Y. Shiau, C. J. Medforth, T. J. Dougherty and K. M. Smith, *Tetrahedron Lett.*, 1990, **31**, 7399; (*e*) R. K. Pandey, F.-Y. Shiau, C. J. Medforth, T. J. Dougherty and K. M. Smith, *Tetrahedron Lett.*, 1990, **31**, 789; (*f*) I. K. Morris and A. D. Ward, *Tetrahedron Lett.*, 1988, **29**, 2501; (*g*) R. K. Pandey and T. J. Dougherty, *Photochem. Photobiol.*, 1988, **47**, 769; (*h*) R. K. Pandey, T. J. Dougherty and K. M. Smith, *Tetrahedron Lett.*, 1988, **29**, 4657; (*i*) A. F. Mironov, A. N. Nizhnik, I. V. Deruzhenko and R. Bonnett, *Tetrahedron Lett.*, 1990, **31**, 6409.
6 R. K. Pandey, K. M. Smith and T. J. Dougherty, *J. Med. Chem.*, 1990, **33**, 2032.
7 R. K. Pandey, M. G. H. Vicente, F.-Y. Shiau, T. J. Dougherty and K. M. Smith, *Proc. SPIE Int. Soc. Opt. Eng.*, 1991, **1426**, 356.
8 (*a*) R. K. Pandey, A. B. Sumlin, W. R. Potter, D. A. Bellnier, B. W. Henderson, S. Constantine, M. Aoudia, M. R. Rodgers, K. M. Smith and T. J. Dougherty, *Photochem. Photobiol.*, 1996, **63**, 194; (*b*) R. K. Pandey, T. Tsuchida, S. Constantine, G. Zheng, C. Medforth, A. Kozyrev, A. Mohammad, M. A. J. Rodgers, K. M. Smith and T. J. Dougherty, *J. Med. Chem.*, 1997, **40**, 3770.
9 B. W. Henderson, D. A. Bellnier, W. R. Graco, A. Sharma, R. K. Pandey, L. Vaughan, K. R. Weishaupt and T. J. Dougherty, *Cancer Res.*, 1997, **57**, 4000.
10 (*a*) T. Ando, K. Irie and K. Kosimizu, *Agric. Biol. Chem.*, 1991, **55**, 2441; (*b*) M. A. F. Faustino, M. G. P. M. S. Neves, M. G. H. Vicente, J. A. S. Cavalerio, M. Neumann, H.-D. Brauer and G. Jori, *Photochem. Photobiol.*, 1997, **66**, 405.
11 J. K. Hoober, T. W. Sery and N. Yamamoto, *Photochem. Photobiol.*, 1988, **48**, 579.
12 B. W. Henderson, S. M. Waldo, T. S. Mang, W. R. Potter, P. B. Malone and T. J. Dougherty, *Cancer Res.*, 1985, **45**, 572.
13 D. Allan, A. A. Gorman, I. Hamblett, B. W. Hodgson and C. Lambert, *Photochem. Photobiol.*, 1993, **57**, 893.
14 J. R. Hurst, J. D. McDonald and G. B. Schuster, *J. Am. Chem. Soc.*, 1982, **104**, 2064.
15 D. D. Perrin, W. L. F. Armarego and D. R. Perrin, *Purification of Common Laboratory Chemicals*, Pergamon Press, Oxford, 1966.
16 W. E. Ford, M. J. Rodgers, L. A. Schechtman, J. R. Sounik, B. D. Rihter and M. E. Kenney, *Inorg. Chem.*, 1992, **31**, 3371.
17 R. Schnidt and E. Afshari, *J. Phys. Chem.*, 1990, **94**, 4377.
18 K. Kalanasundra and M. Gratzel, *Helv. Chim. Acta*, 1980, **63**, 478.
19 J. N. Demas and G. A. Crosby, *J. Phys. Chem.*, 1971, **75**, 991.
20 K. Chattopasundaram, C. V. Kumar and P. K. Das, *J. Photochem.*, 1984, **24**, 1.